Annealing steel coils

Mark McGuinness
Victoria University of Wellington

Winston Sweatman
Massey University

Duangkamon Baowan
University of Wollongong

Steve Barry
University of New South Wales @ADFA

Abstract

Cold rolled steel in the form of coiled sheets requires heat treatment (annealing) in order to release stresses and reform the crystalline structure. During this process the whole coil must be heated to the required temperature and then maintained at this temperature for a period of time. At New Zealand Steel the process takes place inside a batch annealing furnace. The MISG group considered the problem of where the cold point lies within the steel coils, i.e. what is the last part of the coil to reach the required temperature, and how long does it take to reach this temperature? Challenges include deciding what the boundary conditions are on a coil, and dealing with the nonlinearity and anisotropy caused by height-dependent gaps within coils.

1 Introduction

During steel manufacture, the process of cold rolling introduces stresses due to changes in the crystalline structure of the metal. These stresses are released by further heat treatment (annealing) which reforms the crystalline structure and reintroduces desirable mechanical properties. The steel for this stage is in the form of a coil. This coil has been produced by wrapping a long steel sheet about an armature, which is then removed, leaving a curved inner surface. The entire steel coil has to be raised to a specified temperature within a *Uniflow Annealing System* (UAS) furnace. The steel coil is then maintained at this temperature for a period of time to achieve annealing.

New Zealand Steel have a number of empirical formulae that they use to decide how long to keep a set of coils in the furnace, to ensure the thermal centre of each coil reaches the desired temperature. These formulae were derived from data generated during commissioning of the furnace, and subsequently lost. The formulae have also been modified over the years, and the original formulae are no longer available.

The following are the objectives identified by the industry representatives:

1. Determine the cold point in a single cold rolled annealed coil taking into account radial and axial heat transfer.

2. Develop new heating formulas based on coil weight, width and thickness if appropriate.

3. Evaluate heating time variation with coil position in the furnace.

During the week some progress was made on addressing both of the first two objectives. The third (extra) objective was also the subject of discussion. A challenging feature of modelling this process remains the practical difficulties encountered in taking experimental measurements within the furnace.

To begin to address the issues, the heat transfer from the furnace through the steel coils must be modelled. We desire to determine the internal point within each coil that takes the longest time to reach the required temperature, and to find how much time is necessary for that to occur. Two parts to the problem can be identified. One is to establish the boundary conditions at the exterior of the steel coils and the other is to model the internal conduction within the steel coils. In both these areas information and insight were provided to the MISG group by the industry representatives and from the literature.

2 Conditions within the UAS furnace

For the New Zealand Steel annealing process, batches of steel coils are placed upon a ventilated steel platform in a single layer on their circular ends (see Figure 1). The ventilation consists of vertical holes that pass completely through the platform. Typically there are nine coils in a square formation on the platform. Each coil weighs between ten and twenty tonnes, is 700 to 1500mm high (this is the width of the steel strip before being coiled), and the steel strips are from 0.4 to 3mm thick.

The ventilated platform is transported through the front door of the furnace to initiate the heating process. After annealing is complete the platform exits at the back of the furnace into another chamber. The furnace is filled with heated gas, an inert mixture of nitrogen (93% by volume) and hydrogen. This is circulated around the coils. Heating is by radiant burners in the ceiling and on the sides of the furnace. The burners at the sides are shrouded so that they do not radiatively heat the coils, but they do heat the gas. The burners in the ceiling are almost uniformly spread over the set of nine coils.

It is difficult to determine exact boundary conditions for the steel coils. There is limited experimental data available and the gathering of such data is difficult. One measurement that has been recorded is the temperature at two points in the furnace: one in contact with the top surface of one of the steel coils and the other directly above this position and within the heated gas. An example of this data is shown in Figure 2.

Considering an individual steel coil, heat transfer is achieved by a mixture of direct radiation from the heaters in the ceiling of the furnace, conduction from the ventilated steel platform below the coils, and convection by the inert gas (nitrogen/hydrogen mixture) which is blown over heaters and around the coils inside the furnace. The measurements in Figure 2 indicate that the temperature on the circular top of the coil is very close to that of the neighbouring gas. This is likely due to rapid direct radiative heating of the top of the coil by the heaters in the ceiling. As a consequence, the upper boundary is here assumed to have a temperature that matches the furnace gas temperature. The circular base of the coil is assigned this temperature too, as the ventilated steel platform with its relatively large surface area is anticipated to heat very rapidly to the gas temperature, and then conduct heat directly into the lower end of each coil. Heating on the curved inner and outer surfaces of a

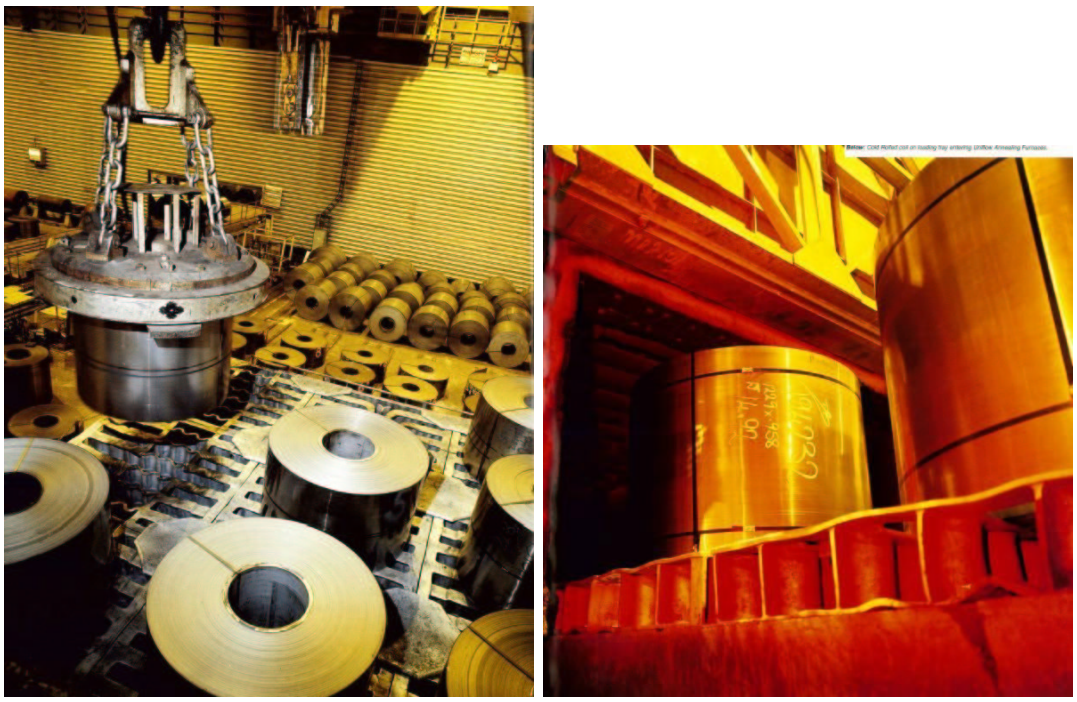

Figure 1: Photographs of steel coils being prepared for and entering the UAS furnace. (Photographs courtesy of NZ Steel.)

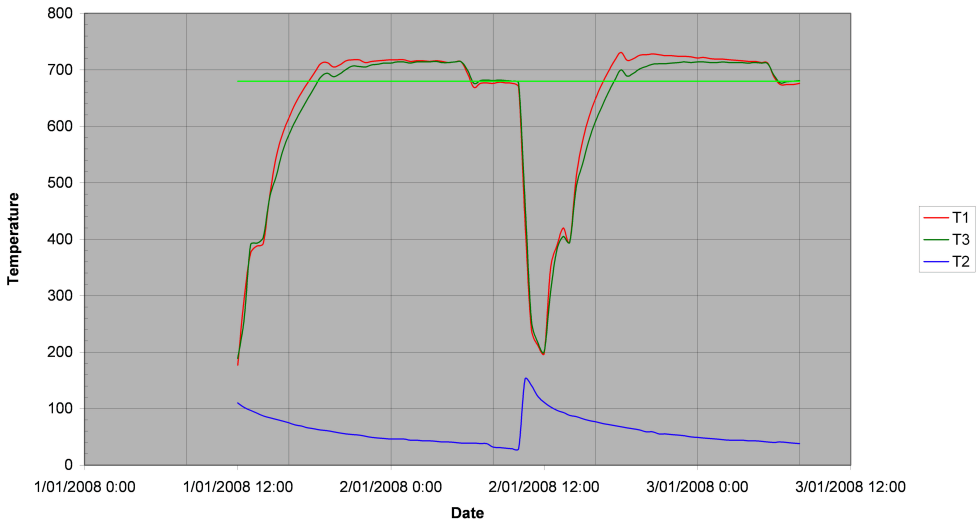

Figure 2: Temperature measurements (°C) taken inside a UAS furnace during just under two heating cycles. The uppermost curve (T1) is the gas temperature above a set of coils, and the curve just below (T3) is the temperature of the upper outer edge of a coil. The target temperature of 680°C is also shown. The lowest line (T2) is the gas temperature in the chamber that the coils are cooled down in following annealing. (Figure courtesy of NZ Steel.)

coil is by convection from the surrounding gas and so the boundary condition here is that of Newton's Law of Cooling.

3 Heat transport within the coils

Superficially, each steel coil can be considered to be a hollow cylinder, annular in cross-section. However, as the coils are rolls of sheets of steel, there are gaps in the radial direction between the neighbouring parts of the steel sheet. As the gas in these gaps has a lower conductivity than steel, the effective conductivity of the coil in the radial direction is lower than that in the vertical direction (within the steel sheet). As a first approximation, the gap between the sheets is assumed to be constant. However, in practice, due to the non-uniformity of the rolling process, the steel sheet has a crown; that is it is thicker in the middle of the sheet than at the edges. This means that the radial gap varies in width vertically along the coil, being larger at the top and bottom ends of the coil, and smaller halfway up, where it is primarily due to surface roughness that there is a gap present. In principle, the thermal conductivity in the radial direction also varies with coil tension and differential heat expansion of the coils due to temperature gradients, and so is dependent on radial position as well as vertical position. When there is contact between the radial steel layers, heat transport could occur through steel-steel contact [6], by diffusion through the gas in the gap, and by radiation across the gap. However, to a reasonable extent, a rough contact surface can still be treated as if it were effectively a small uniform width gap [10, 9].

Therefore, since the number of windings in each one is large, we model a coil as a uniform hollow cylinder with radial conductivity dependent on position:

$$\frac{\partial(c_p \rho T)}{\partial t} = \frac{1}{r}\frac{\partial}{\partial r}\left(k_r r \frac{\partial T}{\partial r}\right) + \frac{\partial}{\partial z}\left(k_z \frac{\partial T}{\partial z}\right) \ , \tag{1}$$

where T [K] is the temperature, c_p [J/kg/K] is the heat capacity which is a function of temperature, ρ [kg/m^3] is the density of the steel, $k_r(z)$ [J/m/s/K] is the radial conductivity, and k_z [J/m/s/K] is the vertical conductivity which is assumed to be the constant conductivity of steel, k_s. The relevant dimensions and properties are listed in Table 1.

3.1 Radial conductivity — Modelling the gaps

In some of the literature [7, 8], the coils are modelled as a concentric series of separate annular cylinders of metal with hot gas between, as illustrated in Figure 3. Then variations in the radial gaps due to crowning (varying strip thickness) and due to temperature gradients inducing differential expansions are calculated [7, 8].

Using the data provided by New Zealand Steel, the geometry is sketched in Figure 4, where lengths, a, b, and d are indicated. Here we use z' to represent the vertical distance from the centre of the coil or equivalently the distance from the centre of the steel sheet towards its edges. The sheets are of a fairly constant thickness at their centre but taper towards the edges. Near the edges, that is the top or base of the coil, the effective radial thermal conductivity is given by

$$k_{\text{eff}} \approx \frac{a+b}{\frac{a}{k_s}+\frac{b}{k_g}} \ , \quad 419.74 \le z' \le 550 \ . \tag{2}$$

steel density	ρ	7854	kg/m^3 (at 300k)
steel thermal conductivity	k_s	60.5	W/m/K at 300K
		56.7	W/m/K at 400K
		48	W/m/K at 600K
		39.2	W/m/K at 800K
		30	W/m/K at 1000K
steel thermal capacity	c_p	434	J/kg/K at 300K
		487	J/kg/K at 400K
		559	J/kg/K at 600K
		685	J/kg/K at 800K
		1169	J/kg/K at 1000K
gas thermal conductivity	k_g	0.06	W/m/K
furnace circulation		800	m^3/minute
steel strip thickness		0.4–3	mm
steel strip width		700–1500	mm
coil mass		10–20	tonnes
coil inner diameter		508	mm
coil outer diameter		1.5	m
platform mass		37	tonnes
furnace dimensions		$6.5 \times 6.5 \times 4$	m^3

Table 1: Table of steel and coil properties.

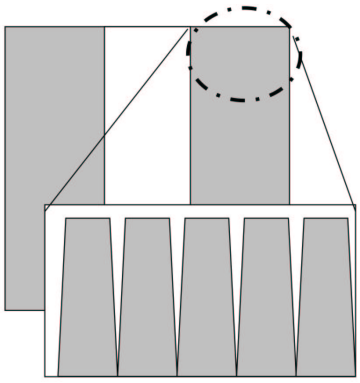

Figure 3: A sketch of the cross section of a coil, with the close up showing how variation in strip thickness causes a variation with height in the gas gap within the coil.

This expression for effective conductivity is only exact for the steady state and the limit of infinite layers [5]. In this z' range,

$$a + b = d\ , \quad b = s(z' - 418.42)\ , \tag{3}$$

where measurements indicate that the slope s is 0.038/50. In the central contact region between the two sheets a 1μm gap (an effective gap due to roughness) gives

$$k_{\text{eff}} \approx \frac{d}{10^{-6}/k_g + (d - 10^{-6})/k_s}\ , \quad z' \leq 419.74\ . \tag{4}$$

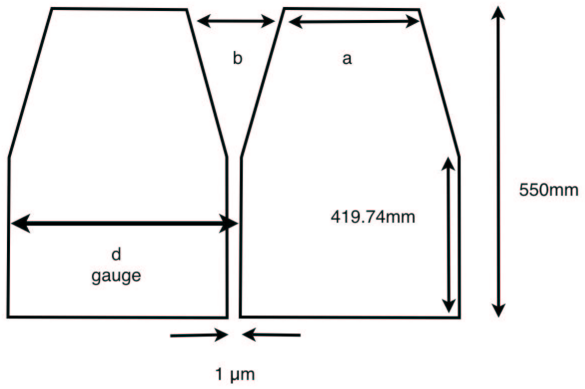

Figure 4: A sketch showing the geometry of the hot gas gap between two sheets of steel in a coil. The sketch shows the upper half of a cross-section through two 1.1m wide sheets.

Using these equations, the effective radial thermal conductivity is in the range 14–25 W/m/K when d is in the range 0.4–3 mm. These thermal conductivities are plotted in Figure 5. Note that these radial thermal conductivities are smaller than the vertical thermal conductivity, $k_s = 30$ W/m/K at 1000K.

If we consider just radial conduction, then the results in Figure 5 indicate that crowning effectively causes an overall reduction in k_r because of the very low radial conduction at the top and bottom of the coils. However, in practice, these ends are heated rapidly by vertical conduction.

3.2 Estimates of heating times

The timescale for heating is

$$t = \frac{\ell^2 \rho c_p}{k}\ , \tag{5}$$

where ℓ is the lengthscale, and k is the appropriate (effective) thermal conductivity. This formula assumes that the surface of the steel is immediately raised to the target temperature. So an approximate estimate of the time to heat a coil of steel, if there is only axial (vertical) heating, is

$$t = 10\text{–}50 \ \text{ hours} \tag{6}$$

for $\ell = 350$–750mm (half the height of a coil) and using $k = k_s$. A solution of the heat equation in the vertical direction with upper and lower surfaces fixed at T_{gas} obtained using Maple, is shown in Figure 6.

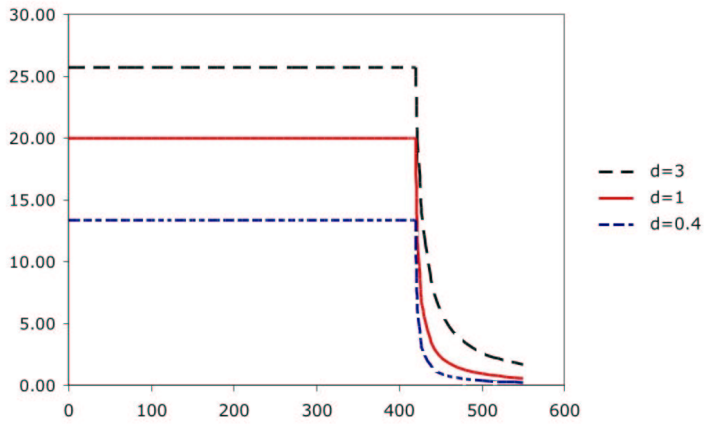

Figure 5: Effective radial thermal conductivities (W/m/K) resulting from the geometry sketched in Figure 4, plotted against vertical distance from the middle of a coil z' (mm), for gauges $d = 0.4$, 1, and 3 mm, and for a temperature of 1000K.

If we consider heating purely in the radial direction, near the centre of the coil, so that $\ell = 250$mm, then the corresponding timescales are

$$\begin{aligned} t &= 12 \text{ hours}, \qquad \text{when } d = 0.4 \text{ mm} \\ t &= 8 \text{ hours}, \qquad \text{when } d = 1 \text{ mm} \\ t &= 6 \text{ hours}, \qquad \text{when } d = 3 \text{ mm} . \end{aligned} \tag{7}$$

However, this does not take into account the restrictive effect of Newton heating on the curved surfaces, discussed in detail in the next section.

3.2.1 Radial boundary condition

Radial heating is driven by conduction from the hot gas rather than by direct radiant heating from the furnace burners. This means that the heating times above need to be reconsidered in light of the heat transfer coefficient H. When they are at temperature T, the heat flux into the (inner and outer) curved surfaces of the coils is

$$Q_c = H(T_{\text{gas}} - T), \quad \text{where} \quad H = \frac{\text{Nu}\, k_g}{D}, \tag{8}$$

and Nu is the Nusselt number (the ratio between actual — convective — heat transfer and that which would be achieved with only conductive processes at work in the hot gas), and D is the hydraulic diameter of the region the hot gas is flowing through. A number of semi-empirical formulae exist for Nu in the case of forced convection, in terms of the Reynolds number Re ($\approx 2.7 \times 10^4$ for the UAS furnace) and the Prandtl number Pr ≈ 0.7, including the laminar flow case:

$$\text{Nu} = 0.648\sqrt{\text{Re}}\,(\text{Pr})^{\frac{1}{3}} , \tag{9}$$

and, in the turbulent flow case, the Dittus-Boelter formula

$$\text{Nu} = 0.023\text{Re}^{0.8}\text{Pr}^{0.3} , \tag{10}$$

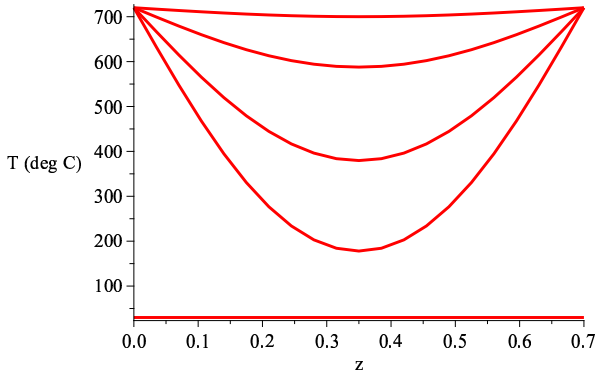

Figure 6: Solutions calculated by Maple to the axial (vertical) heating problem, using $k_s = 30$ W/m/K, $c_p = 1169$ J/kg/K, $T = 720°$C top and bottom, and initial temperature 30°C. The different curves show temperatures (°C) at 0, 2, 4, 8 and 16 hours plotted against vertical distance z (m) from the bottom of the steel coil: the lowest curve is the temperature in the coil at time zero; the uppermost curve is the temperature in the coil after 16 hours of heating when this temperature is everywhere close to 720°C.

and the Gnielinski formula

$$\mathrm{Nu} = \frac{0.037\mathrm{Re}^{0.8}}{1 + 2.443\mathrm{Re}^{-0.1}(\mathrm{Pr}^{2/3} - 1)} \ . \tag{11}$$

All of these formulae give values for H in the range 3–5.

The question addressed here is whether the rate of heat transfer from the hot gas is the main limitation, or the rate at which heat is conducted radially into the steel coil from its surface. The Biot number helps answer this, since it is the ratio of the heat transfer rate at the surface to the heat transfer rate inside the coil:

$$\mathrm{Bi} = \frac{H\ell}{k_s} \approx 0.1 \ . \tag{12}$$

This value being much less than 1 indicates that the rate-limiting factor for radial heat transfer, is heat transfer from the hot gas to the surface of the coil, rather than within the coil. This calculation is supported by numerical solutions to the radial heat equation using Maple, illustrated in Figure 7. In this figure, the internal temperatures stabilise much faster than the overall temperature rises.

The exact details of how the radial thermal conductivity varies with height and with temperature gradients are of less importance than the details of the heat transfer process, across a thermal boundary layer in the hot gas, into the curved vertical surfaces of a coil. Heat transfer in the vertical direction is much more rapid, despite the longer distances involved, because radiation from above and the ventilated platform from below are far more effective at heating the horizontal surfaces.

Furthermore, discussion with the industry representatives suggested that the tensions and roughness of the actual coils would tend to reduce the variations with temperature gradient. Hence we now consider a model in which the horizontal cross-section of the coil is effectively concentric annuli of metal and gas that remain constant in size.

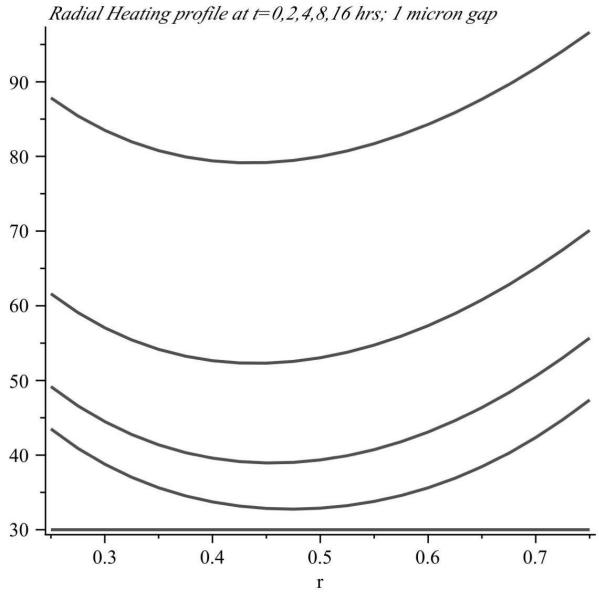

Figure 7: Solutions calculated by Maple to the radial heating problem, using $H = 5$ in the flux boundary condition, $k_s = 20$ W/m/K, $c_p = 1169$ J/kg/K, $T_{\text{gas}} = 720°$C, and initial temperature 30°C. Temperature (°C) is plotted against radial distance (m) from the centre of the annulus that is the cross-section of the steel coil. Time zero is the lowest curve; 16 hours of heating is the uppermost curve. Note the relatively slow rise in boundary temperatures. Also note that the coldest point is nearer the inner face of the coil, due to its smaller surface area (hence smaller heat flux).

4 Linear heat transfer — analytic solutions

In this section we find analytic solutions for linear heat transport within a cylindrical shell. This allows us to consider both radial and axial heat flow simultaneously.

We assume that the coil is a homogeneous region, although with anisotropic heat conductance, so that k_r and k_z are constant. The coordinate system is shown in Figure 8. The solution takes the form of a series whose leading order behaviour is governed by a dominant eigenfunction.

In the linear model, (1) is written in the simpler form

$$\frac{\partial T}{\partial t} = D_r \frac{1}{r}\frac{\partial}{\partial r}\left(r\frac{\partial T}{\partial r}\right) + D_z \frac{\partial}{\partial z}\left(\frac{\partial T}{\partial z}\right). \tag{13}$$

Our boundary and initial conditions are

$$k_r \frac{\partial T}{\partial r} = H(T - T_g), \quad \text{at } r = a, \quad k_r \frac{\partial T}{\partial r} = -H(T - T_g), \quad \text{at } r = b, \tag{14}$$

$$T(r, z = 0, t) = T(r, z = L, t) = T_g, \quad T(r, z, t = 0) = T_0, \tag{15}$$

where $D_r = k_r/(\rho c_p)$, $D_z = k_z/(\rho c_p)$ are assumed constants, T_g is the external gas temperature, and T_0 the initial temperature of the coil. These equations are scaled using typical

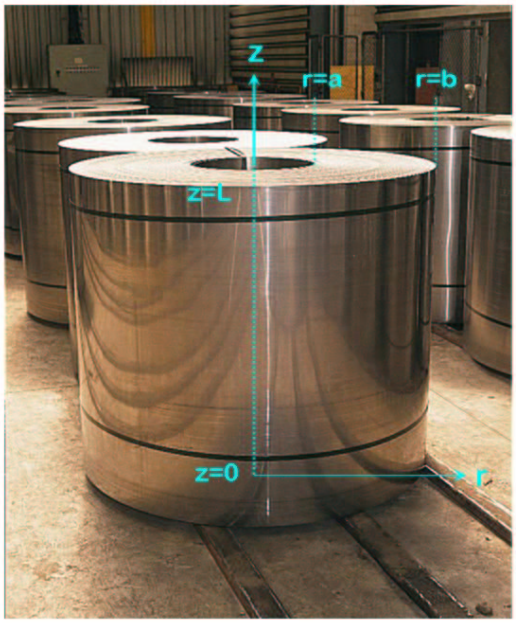

Figure 8: The coordinate system of a coil of height $z = L$ and radius $r \in [a, b]$. (Photograph courtesy of NZ Steel.)

values, $t = t_0, r = b, z = L, T = T_g$:

$$t = t_0 t^*, \quad r = b r^*, \quad z = L z^*, \quad u = \frac{T - T_g}{T_0 - T_g}, \tag{16}$$

where r^*, z^*, t^*, u are the non-dimensional variables. There is a choice of two obvious time scales t_0, using either D_r or D_z. For the problem of interest it is not clear which is dominant and they are of similar magnitude. Hence, without loss of generality we take

$$t_0 = \frac{L^2}{D_z}.$$

The linearised, non-dimensional system is thus

$$\begin{aligned} &\frac{\partial u}{\partial t} = D \frac{1}{r} \frac{\partial}{\partial r} \left(r \frac{\partial u}{\partial r} \right) + \frac{\partial^2 u}{\partial z^2}, \\ &\frac{\partial u}{\partial r} = hu, \quad \text{at} \quad r = a, \quad \frac{\partial u}{\partial r} = -hu, \quad \text{at} \quad r = 1, \\ &u(r, z = 0, t) = u(r, z = 1, t) = 0, \quad u(r, z, t = 0) = 1, \end{aligned} \tag{17}$$

where the * notation has been dropped for convenience, $D = D_r L^2 / D_z b^2$ represents the relative diffusivity, $a \in [0, 1]$ (strictly a^*) is the ratio of original lengths a/b, and $h = Hb/k_r$. This equation now represents non-dimensional cooling of a unit cylinder from initial unit temperature to surrounding temperature zero.

The solution is found by separation and Sturm-Liouville theory. A similar solution for the purely radial case can be found, without derivation, in [3] (page 530). Setting

$$u(r,z,t) = R(r)Z(z)T(t) \tag{18}$$

gives

$$\begin{aligned} Z'' &= \mu Z, \quad Z(0) = Z(1) = 0 && (19)\\ R'' + \frac{1}{r}R' &= \omega R, \quad R'(a) = h\,R(a), \quad R'(1) = -h\,R(1) && (20)\\ T' &= (D\omega + \mu)T, && (21) \end{aligned}$$

where ω and μ are members of infinite sets of eigenvalues. The respective eigenfunction solutions are

$$\begin{aligned} Z &= \sin n\pi\, z, \quad \mu = -(n\pi)^2, \quad n = 1, 2, \ldots && (22)\\ R &= C_0(\lambda r) \equiv J_0(\lambda r) + B\,Y_0(\lambda r), \quad \omega = -\lambda^2, && (23)\\ T &= \exp(-(D\lambda^2 + (n\pi)^2)\,t), && (24) \end{aligned}$$

where B is a constant, and J_0, Y_0 are zeroth order Bessel functions. The boundary conditions at $r = a$ and $r = 1$ give

$$\begin{aligned} -\lambda J_1(\lambda a) - B\lambda Y_1(\lambda a) - hJ_0(\lambda a) - hBY_0(\lambda a) &= 0, && (25)\\ -\lambda J_1(\lambda) - B\lambda Y_1(\lambda) + hJ_0(\lambda) + hBY_0(\lambda) &= 0. && (26) \end{aligned}$$

These have a consistent solution for B when

$$\begin{vmatrix} \lambda J_1(\lambda a) + hJ_0(\lambda a) & \lambda Y_1(\lambda a) + hY_0(\lambda a) \\ -\lambda J_1(\lambda) + hJ_0(\lambda) & -\lambda Y_1(\lambda) + hY_0(\lambda) \end{vmatrix} = 0. \tag{27}$$

This characteristic equation can be solved numerically to find λ, as illustrated in Figure 9 for the case $a = 1/3$ and $h = 1$.

Using (18) the full solution is

$$u(r,z,t) = \sum_{n=1}^{\infty}\sum_{m=1}^{\infty} A_{mn}\; e^{-(D\lambda_m^2 + (n\pi)^2)t}\;\; \sin n\pi z\;\; C_0(\lambda_m r), \tag{28}$$

where from (26)

$$B = -\;\frac{hJ_0(\lambda) - \lambda J_1(\lambda)}{hY_0(\lambda) - \lambda Y_1(\lambda)}, \tag{29}$$

and A_{mn} are constants found by Sturm Liouville orthogonality as

$$A_{mn} = \frac{\int_0^1 \sin(n\pi z)dz}{\int_0^1 \sin^2(n\pi z)\,dz}\;\;\frac{\int_a^1 rC_0(\lambda_m r)\,dr}{\int_a^1 rC_0^2(\lambda_m r)\,dr}. \tag{30}$$

These integrals can be evaluated to give

$$A_{mn} = 2\frac{(1-(-1)^n)}{n\pi}\;\;\frac{\left[\frac{r}{\lambda_m}C_1(\lambda_m r)\right]_a^1}{\left[\frac{r^2}{2}\left(C_0^2(\lambda_m r) + C_1^2(\lambda_m r)\right)\right]_a^1} \tag{31}$$

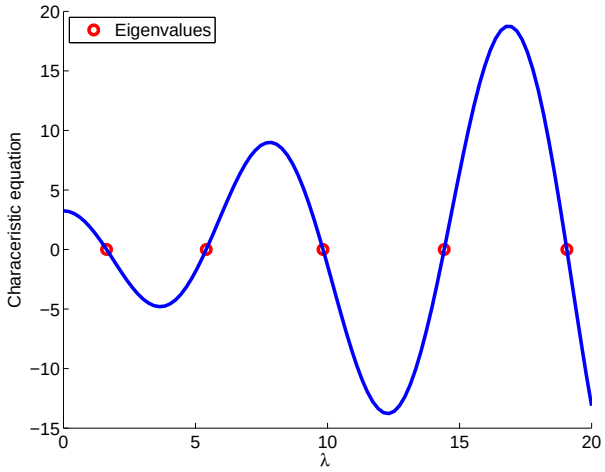

Figure 9: First five eigenvalues shown as zeros of equation (27) for $h = 1$ and $a = 1/3$.

where C_0 and C_1 are given by (23). Use has been made of results from [1](chapters 9 and 11) summarised here using $\mathcal{C}_\nu$ and $\mathcal{D}_\nu$ to represent either J_ν or Y_ν:

$$\mathcal{C}_0'(x) = -\mathcal{C}_1(x) \tag{32}$$

$$\int_a^1 r\mathcal{C}_0(\lambda r)\,dr = \left[\frac{r}{\lambda}\mathcal{C}_1(\lambda r)\right]_a^1 \tag{33}$$

$$\int r\,\mathcal{C}_0(\lambda r)\mathcal{D}_0(\lambda r)\,dr = \frac{r^2}{2}(\mathcal{C}_0(\lambda r)\,\mathcal{D}_0(\lambda r) + \mathcal{C}_1(\lambda r)\,\mathcal{D}_1(\lambda r)). \tag{34}$$

The solution given by (28) can be evaluated to any degree of accuracy at any point using simple numerical summation. However, the dominant behaviour is given by the leading eigenvalues λ_1 and π. In Figure 9 the eigenvalues are shown as zeros of the characteristic equation (27) with $a = 1/3$ and $h = 1$. Numerically they can be shown to asymptote to being $3\pi/2$ apart.

Figure 10 shows the full solution $u(r, z = 0.5, t = 0.04)$ and the leading eigenfunction, equation (23) with $\lambda = \lambda_1$, using scaled values $h = 1$, $D = 1$, and $a = 1/3$. This illustrates that the leading eigenfunction dominates the solution and that the position of the cold point, $r = r_c$, can be given by finding the maximum of this eigenfunction. The time dependence is then governed by the time decay of the exponential term $\exp(-(D\lambda_1^2 + \pi^2)t)$.

Figure 11 shows the dependence of the cold point position and leading eigenvalue as a function of the scaled surface transfer coefficient h with $a = 1/3$, which is comparable to the practical application. Note that the cold point does not vary considerably with h. As h becomes small, the leading eigenvalue becomes small compared with π, the dominant eigenvalue in the z direction; for small h the sides are effectively insulating and diffusion is dominated by the z dependence.

Figure 12 shows a contour plot of the leading eigenvalue as a function of the two parameters governing this variable, h and a. For this application it is unlikely that a will be varied, but this result is included for completeness.

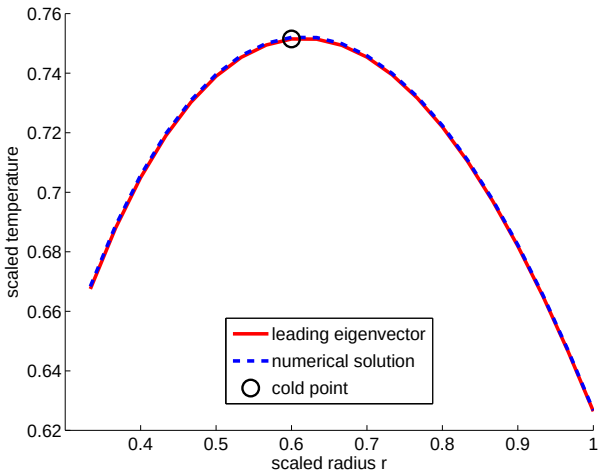

Figure 10: Comparison of full solution $u(r, z = 0.5, t = 0.04)$ and leading eigenfunction (23) for $h = 1$ and $a = 1/3$ with the cold point shown. Hence this eigenfunction is a good predictor of cold point position.

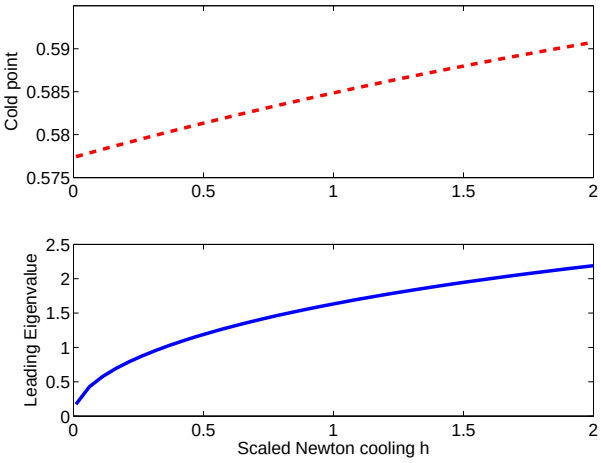

Figure 11: Dependence of the cold point position, $r = r_c$ and leading eigenvalue as functions of scaled surface transfer coefficient h with $a = 1/3$.

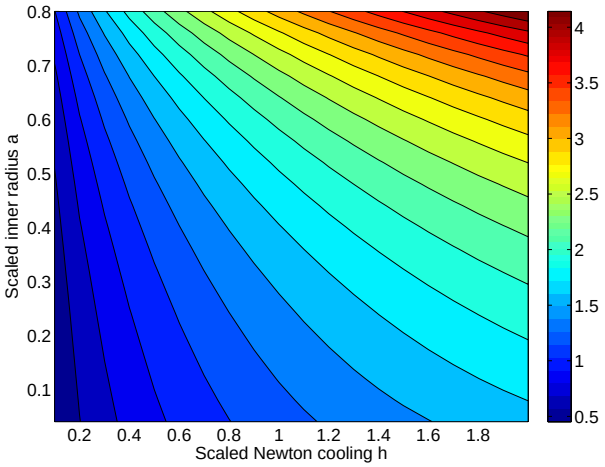

Figure 12: Contour plot showing the dependence of the leading eigenvalue as a function of scaled surface transfer coefficient h and scaled inner width a.

4.1 Implications for heating times

The key feature of the dominant leading term in the solution (28) is the decay in time factor, which in dimensional terms is

$$\exp\left(-\left(\lambda_1^2\frac{D_r}{b^2}+\pi^2\frac{D_z}{L^2}\right)t\right)\ . \tag{35}$$

The first part of the exponent is due to radial heating, the second part is due to axial heating. As noted previously, since the ratio

$$\frac{\lambda_1^2 D_r L^2}{\pi^2 D_z b^2} \tag{36}$$

is approximately 0.1 (using $\lambda_1 \approx 1$), radial heating is much slower than axial heating. However, the effects as evidenced by the exponential decay term above, are multiplicative. For example, increasing the convective transfer term H by a factor of 5 increases the eigenvalue λ_1 by a factor of 2, and this changes the heating time from a scaled value of 0.98 to 0.89, a 10% improvement.

For the cold point to reach the desired soak temperature of 680°C when gas temperature is 710°C and initial temperature is 30°C, the scaled solution u needs to change from the initial value of 1, to the value 30/680. If we ignore radial heating, this happens at the time

$$t=\frac{L^2}{\pi^2 D_z}|\ln(3/68)| \approx 0.32\frac{L^2}{D_z} \approx 1.28\frac{\ell^2}{D_z}\ . \tag{37}$$

This formula reduces by 10% if radial heating is included, to give

$$t \approx 1.15\frac{\ell^2}{D_z}\ . \tag{38}$$

This is almost the same formula as that used in Section 3.2, and gives similar heating times. These results (37) and (38) were checked numerically by setting $u = u_c$ in (28) with $r = r_c$ and $z = 1/2$, where r_c is the cold point established from the leading eigenfunction (20).

5 Numerical solutions

In this section we explore numerical solutions to (1). For the steel coil application we assume that $k_r = k_r(z)$ so that the radial conductivity across the coil is height dependent. We further consider k_z to be constant, ρ to be constant and c_p to be temperature dependent. Using essentially the same non-dimensionalisation system as with the linear solution, with the timescale $t_0 = L^2/(k_z/\rho c_p(1))$, we can write the governing equation as

$$\frac{\partial u}{\partial t} = D_r^* \frac{1}{r}\frac{\partial}{\partial r}\left(r\frac{\partial u}{\partial r}\right) + D_z^* \frac{\partial^2 u}{\partial z^2} - (u + T_1)\frac{\partial \ln c_p}{\partial t} \tag{39}$$

with boundary and initial conditions the same as in (17) and

$$D_r^*(z,u) = \frac{c_p(1)}{c_p(u)}\,\frac{k_r(z)}{k_z}\,\frac{L^2}{b^2}, \quad D_z^*(u) = \frac{c_p(1)}{c_p(u)}, \quad T_1 = \frac{T_g}{T_0 - T_g}. \tag{40}$$

The cumbersome nature of this equation is due to the height dependence $k_r = k_r(z)$ and temperature dependence $c_p = c_p(u)$. If this is relaxed so that k_r and c_p are constant then equation (17) is recovered exactly.

Using second order, central finite differences, the fully nonlinear version of (39) was solved numerically with MATLAB. These experimental results were compared with the analytic solution of Section 4 and found to be accurate for a range of parameter values. Tests for stability and invariance under differing space and time steps were successful.

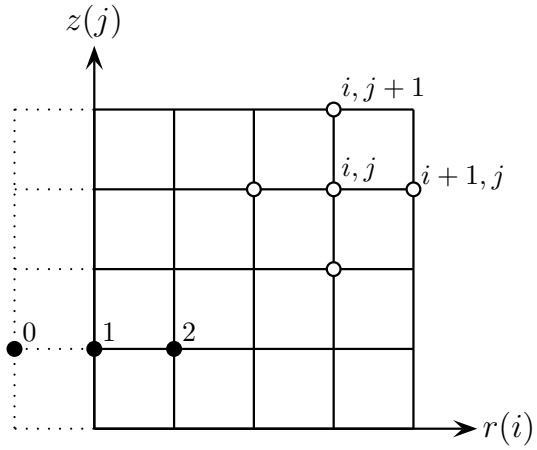

Figure 13: Finite differencing at a central point (i, j) and at a boundary point where a fictitious point is used.

The discretisation used can be illustrated by considering the numerical strategy specifically applied to (17), where c_p is assumed constant. If $u(i\,dr, j\,dz, k\,dt) \equiv u_{i,j}^k$ represents the temperature at discretized position and time then

$$u_{i,j}^{k+1} = u_{i,j}^k + dt\left[D\left(\frac{\partial^2 u}{\partial r^2} + \frac{1}{r}\frac{\partial u}{\partial r}\right) + \frac{\partial^2 u}{\partial z^2}\right], \tag{41}$$

$$\frac{\partial^2 u}{\partial z^2} = \frac{u_{i,j+1}^k - 2u_{i,j}^k + u_{i,j-1}^k}{dz^2}, \tag{42}$$

$$\frac{\partial^2 u}{\partial r^2} = \frac{u^k_{i+1,j} - 2u^k_{i,j} + u^k_{i-1,j}}{dr^2}, \quad \frac{\partial u}{\partial r} = \frac{u^k_{i+1,j} - u^k_{i-1,j}}{2dr}. \tag{43}$$

The discretisation is shown in Figure 5. The boundaries $z = 0$ and $z = 1$ are easily defined by setting $u = 0$. On the boundaries $r = a$ and $r = 1$ we use a fictitious point outside of the region which is then eliminated by combining the discretisation above with the discretized boundary condition. Hence at $r = a$ we use the governing equation and boundary condition in (17) and rearrange to find $u^k_{1,j}$:

$$\frac{u^k_{2,j} - u^k_{0,j}}{2dr} = hu^k_{1,j}, \tag{44}$$

$$u^{k+1}_{1,j} = u^k_{1,j} + dt\left[D\left(\frac{\partial^2 u}{\partial r^2} + \frac{1}{r}\frac{\partial u}{\partial r}\right) + \frac{\partial^2 u}{\partial z^2}\right], \tag{45}$$

with the $\frac{\partial^2 u}{\partial r^2}$ and $\frac{\partial u}{\partial r}$ terms involving $u^k_{1,j}$, $u^k_{2,j}$ and the fictitious point $u^k_{0,j}$. Using (44) to replace $u^k_{0,j}$ in (45) gives the new updated value for $u^{k+1}_{1,j}$. This is similarly applied at $r = 1$.

The numerical solution was found to be sufficiently accurate with a spatial discretisation of 21 points in both r and z directions — although a finer grid size of 41 points was necessary for small values of h. The time step was chosen to minimise computational time while remaining within the stability condition

$$dt < \frac{dx^2}{2D} \tag{46}$$

for all the typical length and diffusion scales in the problem. This numerical solution was also used to find estimates for how many terms are required in the numerical evaluation of the series in (28). As expected, for early times more terms are needed, although 10 terms is usually sufficient for accuracy. At later times, as the exponential term decays more rapidly, less terms are needed.

Figure 14 shows a contour plot of temperature in a cross section of the cylinder, with scaled $h = 0.3$, $t = 0.04$, $a = 1/3$, scaled diffusivity $D = 1/2$ and c_p a constant. These parameter values were chosen to represent realistic values for the coiled steel problem.

Figure 15 shows a cross section of the temperature at $r = 2/3$ with the same parameters as Figure 14. Radial diffusivity is likely to vary with height because of crowning: the uneven thickness across the original cold rolled steel sheets. To investigate this effect, two different solutions are compared, one with the radial diffusivity constant and the other when it varies quadratically as shown on Figure 16. There is very little difference between the solutions. This is because the radial heat transport is so restricted by the surface heat transfer coefficient that heat is predominantly diffused vertically. This is also clear from Figure 14.

6 Variable Diffusivity

The diffusivities that have been used in previous sections to estimate heating times have been based on the properties of steel at 1000K. However, steel diffusivity varies with temperature, and is larger at smaller temperatures, so that we have overestimated heating times. The concept of mean action time [4] allows us to calculate by what factor we have overestimated heating time, by considering that the appropriate average diffusivity to take is

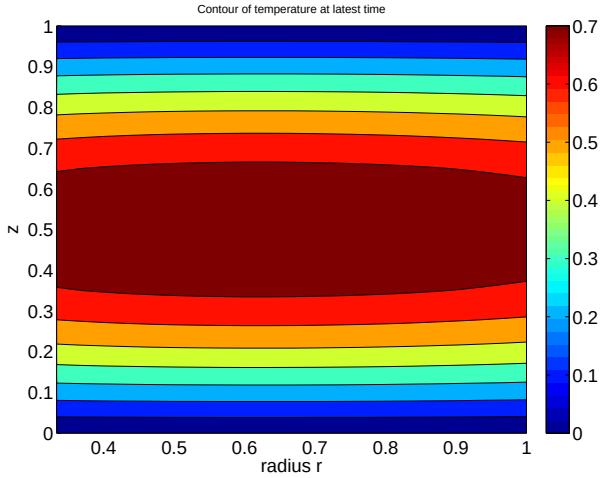

Figure 14: Contour plot of temperature in a cross section of the cylinder, with scaled $h = 0.3$, $t = 0.04$, $a = 1/3$ and scaled diffusivity $D = 1/2$.

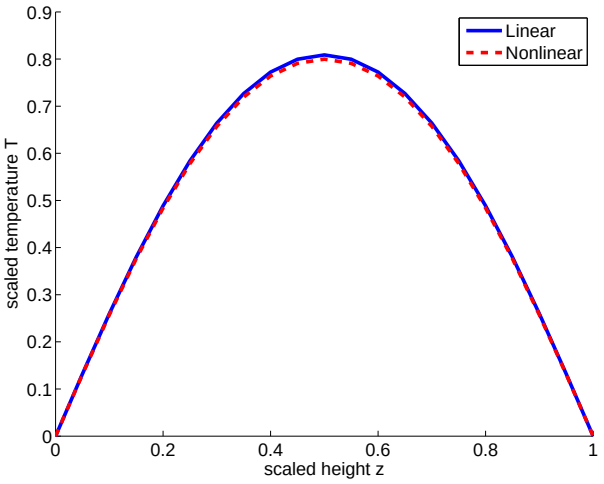

Figure 15: Scaled temperature at $r = 2/3$ versus height with the same parameters as Figure 14. This shows that for Newton cooling on the radial surfaces, varying radial diffusivity has little impact.

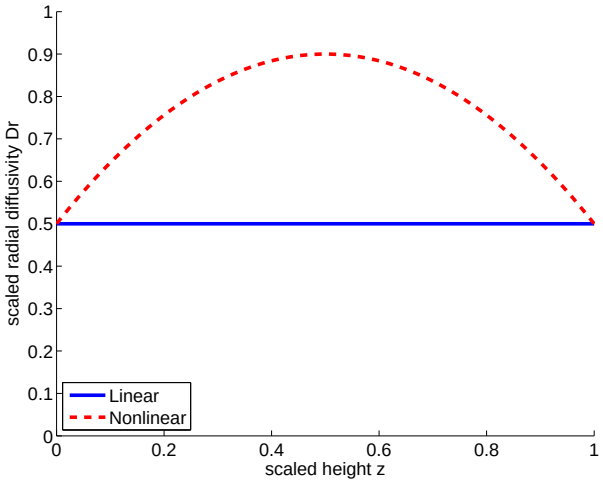

Figure 16: Variation of radial diffusivity with height used in Figure 15 .

$$D_{\text{effective}} = \frac{\int_{T_0}^{T_g} D(T)\, dT}{T_g - T_0} \,. \tag{47}$$

Graphing tabled values of $D(T)$ and fitting a quadratic (using Maple) as illustrated in Figure 17 gives (for T in Kelvin)

$$D \approx 2 \times 10^{-5} - 2.5 \times 10^{-8} T + 4 \times 10^{-12} T^2 \;\; m^2/s \tag{48}$$

and $D_{\text{effective}} \approx 1 \times 10^{-5} \;\; m^2/s$, which is a factor of three larger than the value of D used at 1000K. Hence our estimates of heating time are anticipated to be a factor of three too high.

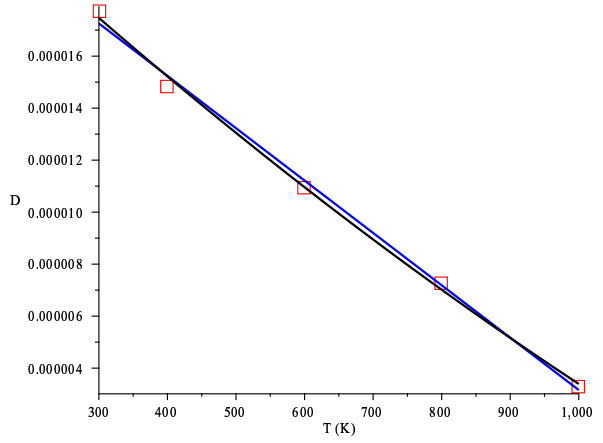

Figure 17: The dependence of diffusivity of steel (m^2/s) on temperature (K), data shown as boxes and a linear and a quadratic fit as curves.

7 Discussion and Conclusions

The analytical and numerical investigations of Sections 4 and 5 suggest that, with the boundary conditions chosen here, the main constriction on the heating of the steel coils is the slow transport of heat through the curved sides of the coils. Further analytical and numerical investigations with radiative heating of all the outer surfaces show a considerable reduction in the heating times [2].

It is difficult without further experimental data to assess the validity of our assumed boundary conditions. We have ignored the effect of the location of the coil in the furnace but industrial experience suggests that failure of the annealing process is associated with particular grid positions within the furnace. There will be further radiation within the furnace such as between the sides of the steel coils. The ceiling plan of the furnace also indicates that some parts of the circular top ends of the coils could be partially shielded from the radiation from above, which would break the cylindrical symmetry which we have assumed. Our modelling underscores the importance of radiative heat transport compared with convective transport.

In any case, our results indicate that the primary variable of concern is the vertical length-scale of the coils, and that considerations such as gauge are secondary, because the radial geometry is in practice independent of gauge, and because radial heat transport is much slower that vertical heat transport. This is because of the boundary conditions rather than the differences in thermal conductivity. Hence, grouping coils by strip width is key to having groups of coils that require the same annealing time in the same batch.

Acknowledgements

We are grateful to the industry representatives Phil Bagshaw, Andrew Mackay and Daniel Yuen for their support and enthusiasm. We also thank the other people who participated in this project who included Seonmin Alm, Barry Cox, Andrew Fowler, Zlatko Jovanoski, Sinuk Kang, Salman Subhani and Ngamta Thamwattana.

References

[1] Abramowitz, M. & Stegun, I. (1970) *Handbook of Mathematical Functions*, Dover, New York.

[2] Barry, S.I., & Sweatman, W.L. (2008) Modelling heat transfer in steel coils, *ANZIAM J (E)*, to appear.

[3] Budak, B.M., Samarskii, A.A., & Tikhonov, A.N. (1964) *A collection of problems in mathematical physics*, Dover, New York.

[4] Landman, K., & McGuinness, M. (2000) Mean Action Time for Diffusive Processes, *J. Appl. Math. Dec. Sc.*, **4**(2), 125–141.

[5] Hickson, R., Barry, S., & Mercer, G. (2008) Heat transfer across multiple layers, *ANZIAM J (E)*, submitted.

[6] Sridhar, M.R., & Yovanovicht, M.M. (1994) Review of elastic and plastic contact conductance models: Comparison with experiment, *J. Thermophysics Heat Transfer*, **8**, 633–640.

[7] Stikker, U.O. (1970) Numerical simulation of the coil annealing process, in *Mathematical Models in Metallurgical Process Development*, Iron and Steel Institute, Special Report **123**, 104–113.

[8] Willms, A.R. (1995) An exact solution of Stikker's nonlinear heat equation, *SIAM J. Appl. Math.* **55**, No. 4, 1059–1073.

[9] Xhang, X., Yu, F., Wu, W., & Zuo, Y. (2003) Application of radial effective thermal conductivity for heat transfer model of steel coils in HPH furnace, *Int. J. Thermophysics* **24**, No. 5, 1395–1405.

[10] Zuo, Y., Wu, W., Zhang, X., Lin, L., Xiang, S., Liu, T., Niu, L., & Huang, X. (2001) A study of heat transfer in high-performance hydrogen Bell-type annealing furnaces, *Heat Transfer — Asian Research*, **30** (8) 615–623.